Harmonic Transfer Function Based Single-input Single-output Impedance Modeling of LCC-HVDC Systems

Yang Wang, Fei Xia, Ying Wang, and Xianyong Xiao

Abstract—**This study presents a harmonic transfer function (HTF) based single-input single-output (SISO) impedance modeling method. The method converts an HTF from phase domain to sequence domain and then transforms it into an SISO impedance while preserving the frequency coupling information of different sequences and different harmonics. Applications of this method to a line-commutated converter based high-voltage direct current (LCC-HVDC) system are presented. The results demonstrate the accuracy of the derived SISO impedance, and a truncation-order selection is suggested. The case study shows that the proposed method facilitates simpler impedance measurements and associated stability analysis.**

Index Terms—**Line-commutated converter based high-voltage direct current (LCC-HVDC), harmonic transfer function (HTF), single-input single-output (SISO) impedance, frequency coupling.**

I. Introduction

THE high penetration of renewables and power electronic devices has raised great concerns on the stability issue [1]-[3]. Compared with the widely-adopted linear time-invariant modeling, the linear time-periodic (LTP) modeling represented by a harmonic state space (HSS) or harmonic transfer function (HTF) is found to be more effective in revealing frequency coupling in the harmonic domain [4]-[7]. However, HTF is multi-input multi-output (MIMO) in nature and thus hinders impedance measurements and impedance-based stability analysis [8], [9].

Recent efforts have been made to convert an MIMO impedance to a single-input single-output (SISO) impedance [10]-[15]. Two-dimensional (2-D) impedences such as the *dq* impedance, sequence impedance, and *αβ*-frame impedance are generally used, and they are proven to be equally valid. Reference [10] developed a generalized method for converting the *dq* impedance model of a grid-tied voltage-source converter (VSC) system into its SISO sequence domain equivalents. In addition, the decoupled SISO model uses the classic Nyquist criterion for stability analysis. However, the 2-D impedances cannot present multi-frequency coupling effects. In [13], an MIMO impedance model of a modular multilevel converter (MMC) was established using an HTF. However, during dimension reduction, only diagonal terms remain, whereas nondiagonal elements are ignored, and this type of dimensionality reduction cannot retain the frequency coupling information. The recent study in [15] proposed a technique to transform the HTF of a single-phase VSC into an SISO impedance model. However, this method does not address the frequency coupling among three phases.

This study extends the method described in [15] to a three-phase system. The first contribution is the proposal of a more generic conversion technique that preserves the frequency coupling information of different sequences and harmonics in a three-phase system. A case study is presented using the CIGRE high-voltage direct current (HVDC) benchmark system. The reason for selecting the line-commutated converter based HVDC (LCC-HVDC) system for demonstration is that some recent works have claimed the importance of HSS modeling for LCC-HVDC systems without sufficient justification [16], [17]. This study attempts to clarify this issue using the derived SISO impedance. This constitutes its second contribution.

II. HSS-based MIMO Impedance Modeling in Sequence Domain

A. Theory of HSS

An LTP system in the time domain can be represented by the state-space model, which is expressed as:

$$\begin{cases} \dot{x}(t)=A(t)x(t)+B(t)u(t) \\ y(t)=C(t)x(t)+D(t)u(t) \end{cases} \tag{1}$$

where $x(t)$ and $u(t)$ are the state and input variables, respectively; $A(t)$, $B(t)$, $C(t)$, and $D(t)$ are the variables in the period of T_0 that satisfy $A(t+T_0)=A(t)$, $B(t+T_0)=B(t)$, $C(t+T_0)=C(t)$, and $D(t+T_0)=D(t)$, respectively; $y(t)$ is the output variable; and $\dot{(\cdot)}$ is the differential symbol.

Based on the Fourier transform, $x(t)$ in the time domain

Manuscript received: February 15, 2023; revised: June 11, 2023; accepted: July 30, 2023. Date of CrossCheck: July 30, 2023. Date of online publication: September 22, 2023.

This work was supported by National Natural Science Foundation of China (No. 52177104).

Y. Wang, F. Xia, Y. Wang (corresponding author), and X. Xiao are with the College of Electrical engineering, Sichuan University, Chengdu 610065, China (e-mail: scufrankwang@163.com; scuerxf@163.com; tuantuan1125@scu.edu.cn; xiaoxianyong@163.com).

DOI: 10.35833/MPCE.2023.000093

can be represented as:

$$x(t)=\sum_{h=-\infty}^{\infty} X_h e^{jh\omega_0 t} \tag{2}$$

where X_h is the h^{th} Fourier coefficient of $x(t)$; and $\omega_0=2\pi/T_0$ is the angular frequency of the fundamental component.

To describe the dynamic characteristics of the system, the exponentially modulated periodic function e^{st} is introduced as the kernel function, and the general form of signal $x(t)$ is given by:

$$x(t)=e^{st}\sum_{h=-\infty}^{\infty} X_h e^{jh\omega_0 t} \tag{3}$$

Substituting (3) into (1), the HSS model of an LTP system can be obtained based on the harmonic balancing principle as [18]:

$$\begin{cases} (s+jh\omega_0)X_h=\sum\limits_{m\in Z} A_{h-m}X_m+\sum\limits_{m\in Z} B_{h-m}U_m \\ Y_h=\sum\limits_{m\in Z} C_{h-m}X_m+\sum\limits_{m\in Z} D_{h-m}U_m \end{cases} \tag{4}$$

where U_m and X_m are the m^{th} Fourier coefficients of signals $u(t)$ and $x(t)$, respectively; Y_h is the h^{th} Fourier coefficient of $y(t)$, and A_{h-m}, B_{h-m}, C_{h-m}, and D_{h-m} are the $(h-m)^{\text{th}}$ Fourier coefficients of signals $A(t)$, $B(t)$, $C(t)$, and $D(t)$, respectively.

The matrix form of (4) can be expressed as:

$$\begin{cases} s\boldsymbol{X}=(\Gamma(\boldsymbol{A})-\boldsymbol{N})\boldsymbol{X}+\Gamma(\boldsymbol{B})\boldsymbol{U} \\ \boldsymbol{Y}=\Gamma(\boldsymbol{C})\boldsymbol{X}+\Gamma(\boldsymbol{D})\boldsymbol{U} \end{cases} \tag{5}$$

$$\begin{cases} \boldsymbol{X}=[\dots \ \ X_{-2}(t) \ \ X_{-1}(t) \ \ X_0(t) \ \ X_1(t) \ \ X_2(t) \ \ \dots]^{\mathrm{T}} \\ \boldsymbol{U}=[\dots \ \ U_{-2}(t) \ \ U_{-1}(t) \ \ U_0(t) \ \ U_1(t) \ \ U_2(t) \ \ \dots]^{\mathrm{T}} \end{cases} \tag{6}$$

where $\boldsymbol{X}$, $\boldsymbol{Y}$, and $\boldsymbol{U}$ are the Fourier coefficients of $x(t)$ and $u(t)$, respectively; $\boldsymbol{N}=\mathrm{diag}(\dots,-j2\omega_0,-j\omega_0,0,j\omega_0,j2\omega_0,\dots)$; $\Gamma(\boldsymbol{A})$, $\Gamma(\boldsymbol{B})$, $\Gamma(\boldsymbol{C})$, and $\Gamma(\boldsymbol{D})$ are the Toeplitz matrices of $\boldsymbol{A}$, $\boldsymbol{B}$, $\boldsymbol{C}$, and $\boldsymbol{D}$, respectively; and the subscripts "+" and "−" represent the positive and negative harmonics, respectively. Taking $\Gamma(\boldsymbol{A})$ as an example, the general form is given by:

$$\Gamma(\boldsymbol{A})=\begin{bmatrix} A_0 & A_{-1} & \cdots & A_{-H} & 0 & \cdots & 0 \\ A_1 & A_0 & \cdots & A_{-H+1} & A_{-H} & \cdots & 0 \\ \vdots & \vdots & & \vdots & \vdots & & \vdots \\ A_H & A_{H-1} & \cdots & A_0 & A_{-1} & \cdots & A_{-H} \\ 0 & A_H & \cdots & A_1 & A_0 & \cdots & A_{-H+1} \\ \vdots & \vdots & & \vdots & \vdots & & \vdots \\ 0 & \cdots & 0 & A_H & A_{H-1} & \cdots & A_0 \end{bmatrix} \tag{7}$$

where H is the order of the harmonic truncation.

B. MIMO Impedance Matrix in Sequence Domain

Once the HSS model of the LTP system is established, the MIMO impedance matrix can be obtained. The purpose of MIMO impedance is to establish the input-output relationship between input harmonic current $\Delta\boldsymbol{I}^{abc}$ and output harmonic voltage $\Delta\boldsymbol{U}^{abc}$. The MIMO impedance matrix in three phases $\boldsymbol{Z}_{\mathrm{HTF}}^{abc}$ can thus be defined as:

$$\Delta\boldsymbol{U}^{abc}=\Delta\boldsymbol{I}^{abc}\boldsymbol{Z}_{\mathrm{HTF}}^{abc} \tag{8}$$

According to the Laplace transform, $\boldsymbol{Z}_{\mathrm{HTF}}^{abc}$ can be calculated by:

$$\boldsymbol{Z}_{\mathrm{HTF}}^{abc}=\Gamma(\boldsymbol{C})(s\boldsymbol{I}-(\Gamma(\boldsymbol{A})-\boldsymbol{N}))^{-1}\Gamma(\boldsymbol{B})+\Gamma(\boldsymbol{D}) \tag{9}$$

where $\boldsymbol{I}$ is the unit matrix.

For a three-phase system, the voltage and current are often described in the sequence domain. Therefore, the symmetric component method is applied to transform $\boldsymbol{Z}_{\mathrm{HTF}}^{abc}$ in the three phases into $\boldsymbol{Z}_{\mathrm{HTF}}^{pn}$ in the sequence domain, as shown by:

$$\begin{bmatrix} \boldsymbol{U}^p \\ \boldsymbol{U}^n \end{bmatrix}=\frac{1}{3}\begin{bmatrix} \boldsymbol{I} & \boldsymbol{\alpha} & \boldsymbol{\alpha}^2 \\ \boldsymbol{I} & \boldsymbol{\alpha}^2 & \boldsymbol{\alpha} \end{bmatrix}\begin{bmatrix} \boldsymbol{U}^a \\ \boldsymbol{U}^b \\ \boldsymbol{U}^c \end{bmatrix} \tag{10}$$

where the superscripts p and n represent the positive and negative sequences, respectively, which represent information related to coupling sequences; and $\boldsymbol{\alpha}=\mathrm{diag}(\dots,e^{j\frac{2}{3}\pi},e^{j\frac{2}{3}\pi},e^{j\frac{2}{3}\pi},\dots)$.

The impedance matrix $\boldsymbol{Z}_{\mathrm{HTF}}^{pn}$ can then be defined as:

$$\begin{bmatrix} \Delta\boldsymbol{U}_{\pm h}^{p} \\ \Delta\boldsymbol{U}_{\pm h}^{n} \end{bmatrix}=\underbrace{\begin{bmatrix} \boldsymbol{Z}_{\pm h,\pm h}^{pp} & \boldsymbol{Z}_{\pm h,\pm h}^{pn} \\ \boldsymbol{Z}_{\pm h,\pm h}^{np} & \boldsymbol{Z}_{\pm h,\pm h}^{nn} \end{bmatrix}}_{\boldsymbol{Z}_{\mathrm{HTF}}^{pn}}\begin{bmatrix} \Delta\boldsymbol{I}_{\pm h}^{p} \\ \Delta\boldsymbol{I}_{\pm h}^{n} \end{bmatrix} \tag{11}$$

where the subscripts (d, q) for each element in $\boldsymbol{Z}_{\mathrm{HTF}}^{pn}$ represent the transfer relationship between the d^{th} output harmonic voltage and the q^{th} input harmonic current, and $d,q\in[-H, H]$.

The frequency coupling of a three-phase system occurs not only under different harmonic frequencies but also under different sequences. $\boldsymbol{Z}_{\mathrm{HTF}}^{pn}$ is a $(4H+2)\times(4H+2)$ matrix. Thus, the dimension of the matrix increases with the harmonic truncation order. A proper truncation order should be selected by striking a balance between accuracy and computational burden.

III. Derivation of SISO Equivalent Impedance Model

A. LCC-HVDC Harmonic Coupling Analysis and Harmonic Truncation Order Selection

The CIGRE HVDC benchmark model [19] is used as an example to explain the derivation of the SISO equivalent impedance model. In Fig. 1, the controllers at the sending and receiving ends are included in the same block, where the variables are marked in red and blue, respectively. All the parameters used are consistent with the benchmark system in [19].

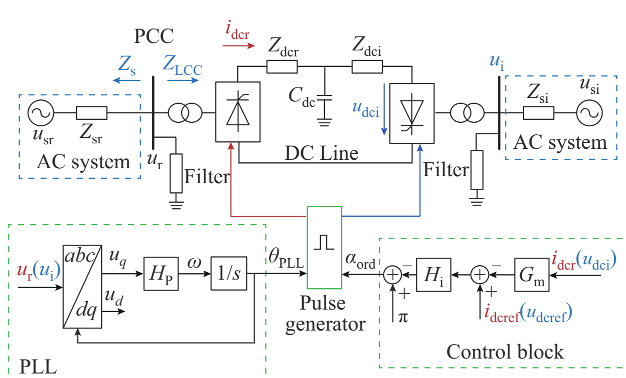

Fig. 1. Schematic of two-terminal LCC-HVDC system.

First, the HSS model of the LCC-HVDC is derived according to [16] and [17]. Then, $\boldsymbol{Z}_{\mathrm{HTF}}^{pn}$ is calculated by (11). Figure 2 shows the magnitude distribution of $\boldsymbol{Z}_{\mathrm{HTF}}^{pn}$ in which the truncation order is 26. Because the magnitude of each element in $\boldsymbol{Z}_{\mathrm{HTF}}^{pn}$ varies with the frequency, it is impossible to show the magnitude distribution for all frequencies. In Fig. 2, the z axis represents the average magnitude of each element in $\boldsymbol{Z}_{\mathrm{HTF}}^{pn}$ in the range of 1-1000 Hz.

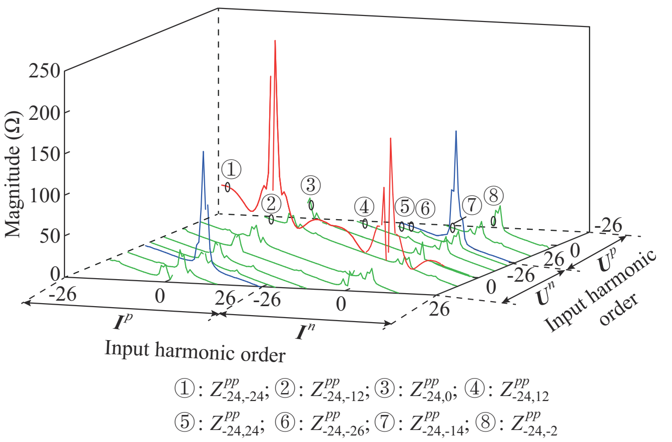

Fig. 2. Magnitude distribution of $\boldsymbol{Z}_{\mathrm{HTF}}^{pn}$ in LCC-HVDC system.

Figure 2 shows that the self- and coupling-impedance exhibit the following features: ① the self-impedance with the input frequency f_{p} is located at the diagonal and has the largest magnitude, as indicated by the red curve; ② the impedances with a frequency of $f_{\mathrm{p}} \pm 2f_0$ are derived from the positive- and negative-sequence coupling and have smaller magnitudes, as indicated by the blue curve; and ③ the impedances with a frequency of $f_{\mathrm{p}} \pm 12kf_0$ and $f_{\mathrm{p}} \pm 2f_0 \pm 12kf_0$ ($k=0,1,2,\ldots$) are derived from the harmonic coupling of the same sequence and have the smallest magnitudes, as indicated by the green curves. It is known that the double-frequency sequence coupling is caused by the asymmetry of the controller in the dq domain. By contrast, the harmonic coupling among the same sequences with much smaller magnitudes is caused by the nonlinear switching dynamics of the converter.

Table I lists the frequency coupling relationships of the impedances, where f_{Ip} and f_{In} are the frequencies of the input current in the positive and negative sequences, respectively; and f_{Up} and f_{Un} are the frequencies of the output voltages in the positive and negative sequences, respectively.

TABLE I
FREQUENCY COUPLING RELATIONSHIPS OF IMPEDANCE

Impedance	Frequency coupling relationship	Impedance	Frequency coupling relationship
$Z^{pp}_{-24,-24}$	$f_{\mathrm{Ip}}=f_{\mathrm{Up}}$	$Z^{pn}_{-24,-26}$	$f_{\mathrm{In}}=f_{\mathrm{Un}}-2f_0$
$Z^{pp}_{-24,-12}$	$f_{\mathrm{Ip}}=f_{\mathrm{Up}}+12f_0$	$Z^{pn}_{-24,-14}$	$f_{\mathrm{Ip}}=f_{\mathrm{Un}}-2f_0+12f_0$
$Z^{pp}_{-24,0}$	$f_{\mathrm{Ip}}=f_{\mathrm{Up}}+2\times 12f_0$	$Z^{pn}_{-24,-2}$	$f_{\mathrm{Ip}}=f_{\mathrm{Un}}-2f_0+2\times 12f_0$
$Z^{pp}_{-24,12}$	$f_{\mathrm{Ip}}=f_{\mathrm{Up}}+3\times 12f_0$	$Z^{pn}_{-24,10}$	$f_{\mathrm{Ip}}=f_{\mathrm{Un}}-2f_0+3\times 12f_0$
$Z^{pp}_{-24,24}$	$f_{\mathrm{Ip}}=f_{\mathrm{Up}}+4\times 12f_0$	$Z^{pn}_{-24,22}$	$f_{\mathrm{Ip}}=f_{\mathrm{Un}}-2f_0+4\times 12f_0$

B. Dimensionality Reduction of MIMO Impedance Matrix

Clearly, the higher the truncation order, the more accurate the impedance model. However, the truncation order cannot be infinite. When the truncation order $H=26$, the order of $\boldsymbol{Z}_{\mathrm{HTF}}^{pn}$ is 106×106. This large matrix leads to a heavy computation burden. According to the previous analysis, the frequency coupling of an LCC-HVDC system includes "$\pm 2f_0$" sequence coupling and "$\pm 12kf_0$" harmonic coupling. When the harmonic coupling is ignored, a truncation order of 3 can be selected. When the harmonic coupling is considered, a truncation order of 13 is sufficient, as higher harmonics have very small magnitudes.

The average magnitude distribution of $\boldsymbol{Z}_{\mathrm{HTF}}^{pn}$ ($H=13$) is shown in Fig. 3 using different colors. When the magnitude is less than 10^{-2}, the element of $\boldsymbol{Z}_{\mathrm{HTF}}^{pn}$ is white. $\boldsymbol{Z}_{\mathrm{HTF}}^{pn}$ is a sparse matrix containing numerous zero elements. Therefore, the dimensions of the impedance matrix can be further reduced without affecting accuracy. The detailed steps are as follows.

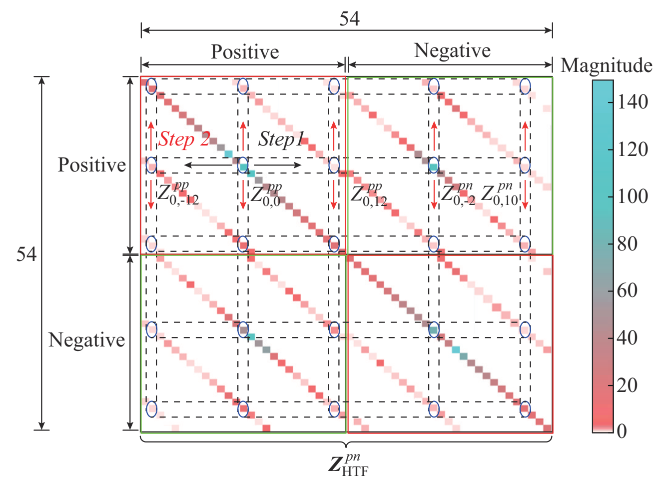

Fig. 3. Dimension reduction of $\boldsymbol{Z}_{\mathrm{HTF}}^{pn}$ based on its average magnitude distribution.

Step 1: when $Z^{pp}_{0,0}$ is selected as the center, the elements in the same row with magnitudes greater than 10^{-2} are extracted. For example, in Fig. 3, $Z^{pp}_{0,-12}$, $Z^{pp}_{0,0}$, $Z^{pp}_{0,12}$, $Z^{pn}_{0,-2}$, and $Z^{pn}_{0,10}$ are extracted.

Step 2: when $Z^{pp}_{0,-12}$, $Z^{pp}_{0,0}$, $Z^{pp}_{0,12}$, $Z^{pn}_{0,-2}$, and $Z^{pn}_{0,10}$ are selected as the center one by one, the elements whose magnitudes are greater than 10^{-2} in the corresponding column are extracted.

Based on these two steps, a new impedance matrix can be obtained, as shown in (12). The dimensions of the MIMO impedance matrix are reduced from 54 to 5.

$$\boldsymbol{Z}_{\mathrm{HTF}}^{pn\prime}=\begin{bmatrix} Z^{pp}_{-12,-12} & Z^{pp}_{-12,0} & Z^{pp}_{-12,12} & Z^{pn}_{-12,-2} & Z^{pn}_{-12,10} \\ Z^{pp}_{0,-12} & Z^{pp}_{0,0} & Z^{pp}_{0,12} & Z^{pn}_{0,-2} & Z^{pn}_{0,10} \\ Z^{pp}_{12,-12} & Z^{pp}_{12,0} & Z^{pp}_{12,12} & Z^{pn}_{12,-2} & Z^{pn}_{12,10} \\ Z^{np}_{-2,-12} & Z^{np}_{-2,0} & Z^{np}_{-2,12} & Z^{nn}_{-2,-2} & Z^{nn}_{-2,10} \\ Z^{np}_{10,-12} & Z^{np}_{10,0} & Z^{np}_{10,12} & Z^{nn}_{10,-2} & Z^{nn}_{10,10} \end{bmatrix} \tag{12}$$

C. Equivalent SISO Impedance Model

To facilitate the impedance measurements and the stability analysis, the MIMO impedance matrix $\boldsymbol{Z}_{\mathrm{HTF}}^{pn\prime}$ should ideally be transformed into SISO impedances Z_{psiso} and Z_{nsiso}, as defined by:

$$\begin{cases} Z_{\text{psiso}} = \Delta U_0^p / \Delta I_0^p \\ Z_{\text{nsiso}} = \Delta U_0^n / \Delta I_0^n \end{cases} \tag{13}$$

where Z_{psiso} and Z_{nsiso} are the positive- and negative-sequence SISO impedances, respectively; ΔU_0^p and ΔI_0^p are the fundamental positive-sequence voltage and current perturbations, respectively; and ΔU_0^n and ΔI_0^n are the fundamental negative-sequence voltage and current perturbations, respectively.

Taking Z_{psiso} as an example, the main objective is to solve the mathematical relationship between ΔU_0^p and ΔI_0^n. The impedance matrix shown in (12) is divided into blocks and rearranged. $Z_{0,0}^{pp}$ in the original matrix is moved to the first position, and the corresponding row and column are moved to the first row and column, respectively, to obtain the new impedance matrix $\boldsymbol{Z}_{\text{HTF}}^{pn\prime\prime}$, as shown by:

$$\begin{bmatrix} \Delta U_0^p \\ \Delta \boldsymbol{U}_{\pm h(h\neq 0)}^p \\ \Delta \boldsymbol{U}_{\pm h}^n \end{bmatrix} = \underbrace{\begin{bmatrix} Z_{0,0}^{pp} & \boldsymbol{Z}_{0,\pm h(h\neq 0)}^{pp} & \boldsymbol{Z}_{0,\pm h}^{pn} \\ \boldsymbol{Z}_{\pm h(h\neq 0),0}^{pp} & \boldsymbol{Z}_{\pm h(h\neq 0),\pm h(h\neq 0)}^{pp} & \boldsymbol{Z}_{\pm h(h\neq 0),\pm h}^{pn} \\ \boldsymbol{Z}_{\pm h,0}^{np} & \boldsymbol{Z}_{\pm h,\pm h(h\neq 0)}^{np} & \boldsymbol{Z}_{\pm h,\pm h}^{nn} \end{bmatrix}}_{\boldsymbol{Z}_{\text{HTF}}^{pn\prime\prime}} \begin{bmatrix} \Delta I_0^p \\ \Delta \boldsymbol{I}_{\pm h(h\neq 0)}^p \\ \Delta \boldsymbol{I}_{\pm h}^n \end{bmatrix} \tag{14}$$

The same operation is performed on the grid side to obtain:

$$\begin{bmatrix} \Delta U_0^{gp} \\ \Delta \boldsymbol{U}_{\pm h(h\neq 0)}^{gp} \\ \Delta \boldsymbol{U}_{\pm h}^{gn} \end{bmatrix} = \underbrace{\begin{bmatrix} Z_{0,0}^{gpp} & \boldsymbol{Z}_{0,\pm h(h\neq 0)}^{gpp} & \boldsymbol{Z}_{0,\pm h}^{gpn} \\ \boldsymbol{Z}_{\pm h(h\neq 0),0}^{gpp} & \boldsymbol{Z}_{\pm h(h\neq 0),\pm h(h\neq 0)}^{gpp} & \boldsymbol{Z}_{\pm h(h\neq 0),\pm h}^{gpn} \\ \boldsymbol{Z}_{\pm h,0}^{gnp} & \boldsymbol{Z}_{\pm h,\pm h(h\neq 0)}^{gnp} & \boldsymbol{Z}_{\pm h,\pm h}^{gnn} \end{bmatrix}}_{\boldsymbol{Z}_{\text{HTF}}^{gpn\prime\prime}} \begin{bmatrix} \Delta I_0^{gp} \\ \Delta \boldsymbol{I}_{\pm h(h\neq 0)}^{gp} \\ \Delta \boldsymbol{I}_{\pm h}^{gn} \end{bmatrix} \tag{15}$$

where the superscript g represents the grid side.

Because the grid impedance is directly connected in series with the LCC-HVDC impedance, additional relationships exist, namely, $\Delta U_0^{gp} = \Delta U_0^p$, $\Delta \boldsymbol{U}_{\pm h(h\neq 0)}^{gp} = \Delta \boldsymbol{U}_{\pm h(h\neq 0)}^p$, $\Delta \boldsymbol{U}_{\pm h}^{gn} = \Delta \boldsymbol{U}_{\pm h}^n$, $\Delta \boldsymbol{I}_{\pm h(h\neq 0)}^{gp} = \Delta \boldsymbol{I}_{\pm h(h\neq 0)}^p$, and $\Delta \boldsymbol{I}_{\pm h}^{gn} = \Delta \boldsymbol{I}_{\pm h}^n$. To simplify the derivation of the SISO impedance, the harmonic components in (14) and (15) are combined and expressed with some symbols, e.g., $[\boldsymbol{Z}_{0,\pm h(h\neq 0)}^{pp}, \boldsymbol{Z}_{0,\pm h}^{pn}]$, is represented by $\boldsymbol{a}$. The simplified formula is given as:

$$\begin{cases} \begin{bmatrix} \Delta U_0^p \\ \Delta \boldsymbol{U}_{\pm h(h\neq 0)}^{p\&n} \end{bmatrix} = \underbrace{\begin{bmatrix} Z_{0,0}^{pp} & \boldsymbol{a} \\ \boldsymbol{b} & \boldsymbol{Q} \end{bmatrix}}_{\boldsymbol{Z}_{\text{HTF}}^{pn\prime\prime}} \begin{bmatrix} \Delta I_0^p \\ \Delta \boldsymbol{I}_{\pm h(h\neq 0)}^{p\&n} \end{bmatrix} \\ \begin{bmatrix} \Delta U_0^{gp} \\ \Delta \boldsymbol{U}_{\pm h(h\neq 0)}^{gp\&gn} \end{bmatrix} = \underbrace{\begin{bmatrix} Z_{0,0}^{pp} & \boldsymbol{a}^g \\ \boldsymbol{b}^g & \boldsymbol{Q}^g \end{bmatrix}}_{\boldsymbol{Z}_{\text{HTF}}^{gpn\prime\prime}} \begin{bmatrix} \Delta I_0^{gp} \\ \Delta \boldsymbol{I}_{\pm h(h\neq 0)}^{gp\&gn} \end{bmatrix} \end{cases} \tag{16}$$

When (16) is solved, the positive-sequence SISO impedance of an LCC-HVDC system can be derived as:

$$Z_{\text{psiso}}(s) = \frac{\Delta U_0^p}{\Delta I_0^p} = \left(1 + \boldsymbol{L}\frac{\boldsymbol{b}^g}{Z_{0,0}^{gpp}}\right)^{-1} (Z_{0,0}^{pp} + \boldsymbol{L}\boldsymbol{b}) \tag{17}$$

$$\boldsymbol{L} = \boldsymbol{a}\left(\frac{\boldsymbol{a}^g \boldsymbol{b}^g}{Z_{0,0}^{pp}} - \boldsymbol{Q}^g - \boldsymbol{Q}\right)^{-1} \tag{18}$$

In many cases, the grid side is assumed to be linear and symmetrical; that is, no coupling occurs in the three phases. This implies that the nondiagonal elements in (15) are all zero. Accordingly, (17) can be simplified as:

$$Z_{\text{psiso}}(s) = Z_{0,0}^{pp} - \boldsymbol{a}(\boldsymbol{Q} + \boldsymbol{Q}^g)^{-1}\boldsymbol{b} \tag{19}$$

It can be observed that the SISO equivalent impedance in the sequence domain contains frequency coupling of different sequences and different harmonics.

IV. SISO Equivalent Impedance Verification and Analysis of System Stability

A. SISO Equivalent Impedance Verification

To verify the accuracy of the derived SISO impedance, the LCC-HVDC system shown in Fig. 1 is built using MATLAB/Simulink, and the impedance is measured by injecting disturbance signals at the point of common coupling (PCC). Figure 4 shows the verification of the SISO impedances Z_{psiso} and Z_{nsiso} under different truncation orders, where $H=1$ denotes the impedance model when no coupling is considered, $H=3$ denotes the impedance model when only sequence coupling is considered, and $H=13$ denotes the impedance model when both sequence and harmonic couplings are considered.

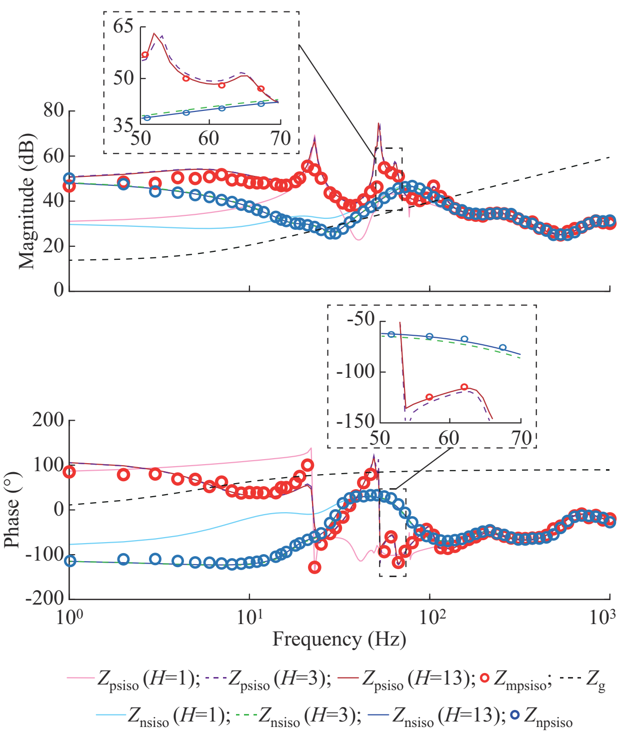

Fig. 4. Impedance models of LCC-HVDC system.

Figure 4 shows that for both positive- and negative-sequence impedances, the case of $H=1$ is completely different from the measured impedance in the low-frequency range because frequency coupling is ignored. In addition, the case of $H=3$ is also close to the measured value, even if its accuracy is not as good as that of $H=13$. Finally, the case of $H=13$ is highly consistent with the measured impedances, thus verifying the correctness of the derived SISO equivalent impedance model.

B. Analysis of System Stability

System stability analysis is conducted using the Nyquist criterion to further demonstrate the effectiveness of the SISO impedance model. The three cases listed in Table II are considered with different proportional coefficients K_{pidc} of the constant-current controller and different truncation orders H.

TABLE II
CASE STUDIES UNDER DIFFERENT K_{pidc} AND H

Case No.	K_{pidc}	H
1	1.0989	3
2	1.6500	3
3	1.6500	13

Based on the assumption that both the LCC-HVDC and power grid can operate stably, the system stability depends on $1+Z_g/Z_{\text{siso}}$ [20]. According to the Nyquist stability criterion, an interactive system is stable if and only if the ratios of positive- and negative-sequence impedances, i. e., $Z_{\text{gp}}/Z_{\text{psiso}}$ and $Z_{\text{gn}}/Z_{\text{nsiso}}$, meet the Nyquist criterion. The instability frequency can be determined based on the frequency of the intersection point between the Nyquist curve of the impedance ratio and the unit circle.

Figure 5 shows the stability analysis results and time-domain verification, where the sampling rate is 20 kHz, and the sampling window is 20 cycles. The red dotted, dashed, and solid lines represent $Z_{\text{gp}}/Z_{\text{psiso}}$ in Cases 1, 2, and 3, respectively. The blue dotted, dashed, and solid lines represent $Z_{\text{gn}}/Z_{\text{nsiso}}$ in Cases 1, 2, and 3, respectively.

Figure 5(a) shows that the Nyquist curve of $\lambda(s)=Z_{\text{gp}}/Z_{\text{psiso}}$ circles (−1, 0) and intersects with the unit cycle at 122 Hz only in Case 3. This means that K_{pidc} changes from 1.0989 to 1.65, resulting in an unstable condition. However, the Nyquist curve of Case 2 does not circle (−1, 0) because of the change in the truncation order from 13 to 3. The simulation results are shown in Fig. 5(b), where K_{pidc} changes from 1.0989 to 1.65 at 1.5 s. The system clearly loses its stability after 1.5 s, and fast Fourier transform analysis of the phase current reveals two oscillation frequencies at 122.5 and 22.5 Hz. This result is thus consistent with that predicted in Case 3, indicating Z_{psiso} ($H=13$) is the most accurate impedance model. No stability issues are observed for the negative sequence, as $Z_{\text{gn}}/Z_{\text{nsiso}}$ does not circle (−1, 0) in all cases.

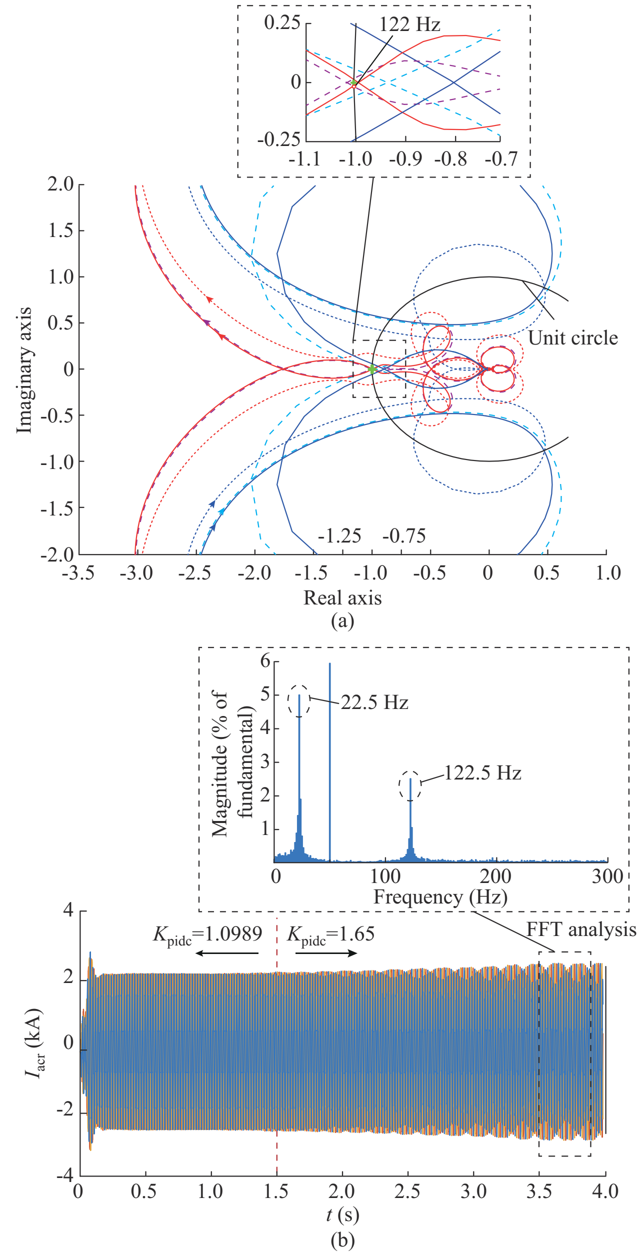

Fig. 5. Stability analysis and time-domain verification. (a) Nyquist curves of $\lambda(s)$ when K_{pidc} changes. (b) Time domain simulation.

V. CONCLUSION

This study presents an HTF-based SISO impedance modeling technique for LCC-HVDC systems. The main purpose of the technique is to analyze frequency-coupling phenomena from a circuit perspective and derive the relationship between the voltage and current at the same frequency. Case studies demonstrate that the derived SISO impedance is very accurate, indicating positive-sequence instability in the simulation study. This also reveals that among different types of frequency couplings, the sequence coupling plays a dominant role in the dynamics of LCC-HVDC systems, whereas the harmonic coupling derived from switching functions can be ignored in most cases. If the latter must be considered to ensure precise stability analysis, a truncation order of 13 is suggested.

REFERENCES

[1] H. Zhang, W. Xiang, W. Lin *et al.*, "Grid forming converters in renewable energy sources dominated power grid: control strategy, stability, application, and challenges," *Journal of Modern Power Systems and Clean Energy*, vol. 9, no. 6, pp. 1239-1256, Nov. 2021.

[2] C. Wan, M. Huang, C. K. Tse *et al.*, "Stability of interacting grid-connected power converters," in *Proceedings of 2014 IEEE International Symposium on Circuits and Systems* (*ISCAS*), Melbourne, Australia, Jun. 2014, pp. 2668-2671.

[3] C. Guo, P. Cui, and C. Zhao, "Optimization and configuration of control parameters to enhance small-signal stability of hybrid LCC-MMC HVDC system," *Journal of Modern Power Systems and Clean Energy*, vol. 10, no. 1, pp. 213-221, Jan. 2022.

[4] C. Zhang, M. Molinas, A. Rygg *et al.*, "Harmonic transfer-function-based impedance modeling of a three-phase VSC for asymmetric AC grid stability analysis," *IEEE Transactions on Power Electronics*, vol. 34, no. 12, pp. 12552-12566, Dec. 2019.

[5] J. Lyu, X. Zhang, X. Cai *et al.*, "Harmonic state-space based small-signal impedance modeling of a modular multilevel converter with con-

sideration of internal harmonic dynamics," *IEEE Transactions on Power Electronics*, vol. 34, no. 3, pp. 2134-2148, Mar. 2019.

[6] R. Pan, G. Tang, S. Liu *et al*., "Impedance analysis of grid forming control based modular multilevel converters," *Journal of Modern Power Systems and Clean Energy*, vol. 11, no. 3, pp. 967-979, May 2023.

[7] H. Zong, C. Zhang, J. Lyu *et al*., "Generalized MIMO sequence impedance modeling and stability analysis of MMC-HVDC with wind farm considering frequency couplings," *IEEE Access*, vol. 8, pp. 55602-55618, Mar. 2020.

[8] V. Salis, A. Costabeber, S. M. Cox *et al*., "Stability assessment of power-converter-based AC systems by LTP theory: eigenvalue analysis and harmonic impedance estimation," *IEEE Journal of Emerging and Selected Topics in Power Electronics*, vol. 5, no. 4, pp. 1513-1525, Dec. 2017.

[9] C. Dang, X. Tong, W. Song *et al*., "Stability analysis of high power factor Vienna rectifier based on reduced order model in *d-q* domain," *Journal of Modern Power Systems and Clean Energy*, vol. 7, no. 1, pp. 200-210, Jan. 2019.

[10] C. Zhang, X. Cai, A. Rygg *et al*., "Sequence domain SISO equivalent models of a grid-tied voltage source converter system for small-signal stability analysis," *IEEE Transactions on Energy Conversion*, vol. 33, no. 2, pp. 741-749, Jun. 2018.

[11] X. Meng, Z. Liu, Y. Liu *et al*., "Conversion and SISO equivalence of impedance model of single-phase converter in electric multiple units," *IEEE Transactions on Transportation Electrification*, vol. 9, no. 1, pp. 1363-1378, Mar. 2023.

[12] J. Guo, Z. Meng, Y. Chen *et al*., "Harmonic transfer-function-based $\alpha\beta$-frame SISO impedance modeling of droop inverters-based islanded microgrid with unbalanced loads," *IEEE Transactions on Industrial Electronics*, vol. 70, no. 1, pp. 452-464, Jan. 2023.

[13] H. Zong, C. Zhang, J. Lyu *et al*., "Block diagonal dominance-based model reduction method applied to MMC asymmetric stability analysis," *IEEE Transactions on Energy Conversion*, vol. 36, no. 3, pp. 2438-2451, Sept. 2021.

[14] J. Lin, M. Su, Y. Sun *et al*., "Recursive SISO impedance modeling of single-phase voltage source rectifiers," *IEEE Transactions on Power Electronics*, vol. 37, no. 2, pp. 1296-1309, Feb. 2022.

[15] C. Zhang, M. Molinas, S. Føyen *et al*., "Harmonic-domain SISO equivalent impedance modeling and stability analysis of a single-phase grid-connected VSC," *IEEE Transactions on Power Electronics*, vol. 35, no. 9, pp. 9770-9783, Sept. 2020.

[16] K. Jiang, P. Hu, K. Cao *et al*., "Small-signal modeling and interaction analysis of LCC-HVDC systems based on harmonic state space theory," *IEEE Access*, vol. 10, pp. 109937-109948, Oct. 2022.

[17] L. Fan, P. Zhou, S. Wang *et al*., "Harmonic state space modeling of LCC-HVDC system with consideration of harmonic dynamics," in *Proceedings of 2019 IEEE 3rd International Electrical and Energy Conference* (*CIEEC*), Beijing, China, Sept. 2019, pp. 2076-2081.

[18] J. Kwon, X. Wang, F. Blaabjerg *et al*., "Frequency-domain modeling and simulation of DC power electronic systems using harmonic state space method," *IEEE Transactions on Power Electronics*, vol. 32, no. 2, pp. 1044-1055, Feb. 2017.

[19] CIGRE Working Group 14.02, "The CIGRE HVDC benchmark model – a new proposal with revised parameters," *Electra*, no. 157, pp. 61-66, Dec. 1994.

[20] J. Sun, "Impedance-based stability criterion for grid-connected inverters," *IEEE Transactions on Power Electronics*, vol. 26, no. 11, pp. 3075-3078, Nov. 2011.

Yang Wang received the B.S. degree in electrical engineering from Zhejiang University, Hangzhou, China, in 2012, and the Ph.D. degree in electrical and computer engineering from the University of Alberta, AB, Edmonton, Canada, in 2017. He is currently a Research Fellow with the College of Electrical Engineering, Sichuan University, Chengdu, China. He is the Editor of the IEEE Transactions on Power Delivery and IEEE Open Access Journal of Power and Energy. His main research interests include power quality and integration of renewable.

Fei Xia received the B.S. degree in electrical engineering from China Three Gorges University, Yichang, China, in 2017. She is currently pursuing the M.S. degree with the School of Electrical Engineering, Sichuan University, Chengdu, China. Her current research interests include modeling and control of power electronic converters, and high-voltage direct current (HVDC) systems.

Ying Wang received the master's degree in signal and information processing and the Ph.D. degree in electrical engineering from Sichuan University, Chengdu, China, in 2007 and 2011, respectively. From 2009 to 2015, she was a Lecturer with Sichuan University, Chengdu, China, where she was an Associate Professor from 2015 to 2021 and has been a Professor since 2021. Her current research interests include voltage sag sensitivity, high-quality power supply and customized power technology, and power quality data mining.

Xianyong Xiao received the Ph. D. degree from Sichuan University, Chengdu, China, in 2010. He is currently a Professor and the Dean with the College of Electrical Engineering and Information Technology, Sichuan University. His research interests include power quality and its control, distribution system reliability, and green friendly smart grid.